
Original Articles

Direct Neural Network Application for Automated Cell Recognition

Qing Zheng,¹ Bruce K. Milthorpe,^{1*} and Allan S. Jones²

¹Graduate School of Biomedical Engineering, University of New South Wales, Sydney, Australia

²Australian Key Centre for Microscopy and Microanalysis, University of Sydney, Sydney, Australia

Received 26 September 2002; Revision Received 21 July 2003; Accepted 4 August 2003

Background: Automated cell recognition from histologic images is a very complex task. Traditionally, the image is segmented by some methods chosen to suit the image type, the objects are measured, and then a classifier is used to determine cell type from the object's measurements. Different classifiers have been used with reasonable success, including neural networks working with data from morphometric analysis.

Methods: Image data of cells were input directly into neural networks to determine the feasibility of direct classification by using pixel intensity information. Several types of neural network and their ability to work with cells in a complex patterned background were assessed for a variety of images and cell types and for the accuracy of classification.

Results: Inflammatory cells from animal biomaterial implants in rabbit paravertebral muscle were imaged in histologic sections. Simple, three-layer, fully connected, back-propagation neural networks and four-layer networks with two layers of a shared-weights neural network were most successful at classifying the cells from the images, with 97% and 98% correct recognition rates, respectively.

Conclusions: The high accuracy recognition rate shows the potential for direct classification of visual image pixel data by neural networks. Cytometry Part A 57A:1-9, 2004. © 2003 Wiley-Liss, Inc.

Key terms: image analysis; neural networks; direct classification

Automating biomaterial histology has been an area for active research since a series of papers published by Mellors between 1951 and 1956 (1-3). Standard manual microscope screening has its limitations: the intense concentration required from the screener, the high cost involved in using and training the expert, and the time of quantification in screening. Thus automatic quantitative analysis is highly desirable.

Many attempts have been made to mimic the procedure of cell recognition from images. Most traditional computerized image analysis systems rely on morphologic segmentation, feature extraction, and classification techniques for cell recognition. In histologic preparations containing debris and synthetic materials, it is difficult to automate cell counting with standard image analysis tools (4).

Artificial neural networks (ANNs) in combination with algorithmic processing and artificial intelligence techniques are emerging software engineering tools for the development of new systems in quantitative cytology and histology from color images. Techniques have been employed for segmentation and pattern recognition (5,6).

ANNs, especially back-propagation neural networks, are widely used for different classification tasks in areas such as remote sensing (7,8), cervical cancer grading (9-12), and flow cytometry (11).

Different cells in microscope images can be differentiated by human visual analysis by using only the spatial and intensity information. The purpose of this study is to introduce several neural network structures and the associated learning procedure for examining the possibility of directly classifying cell types from image input pixel data rather than using standard image analysis methods to derive morphologic parameters. Most of the current applications of neural networks in cell classification from literature rely on the extracted morphologic parameters (13,14). For example, for assessment of bronchial inflam-

*Correspondence to: Bruce K. Milthorpe, Graduate School of Biomedical Engineering, University of New South Wales, Sydney, NSW 2052, Australia.

E-mail: b.milthorpe@unsw.edu.au

Published online in Wiley InterScience (www.interscience.wiley.com). DOI: 10.1002/cyto.a.10106

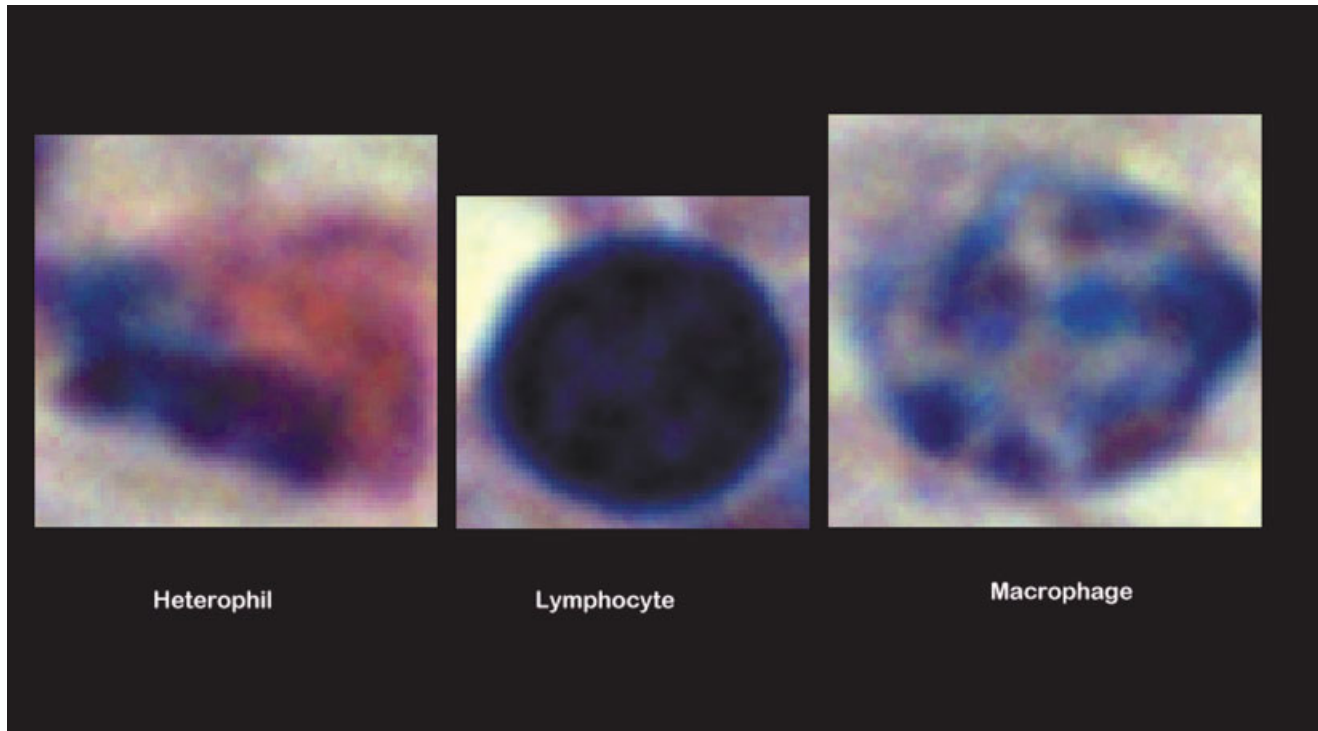


FIG. 1. The three major types of inflammatory cells from rabbit back muscle found in the sample histology. Individual cell images were cropped from the original and are about 50 to 100 pixels across depending on cell size. [Color figure can be viewed in the online issue, which is available at www.interscience.wiley.com.]

mation, Berger et al. (13) developed an automated cell recognition system based on color analysis. Three independent criteria (optic density, hue density, and hue) combined with morphologic parameters were used to recognize a positive staining cell.

It is hypothesized that cells may be directly classified by using back-propagation neural networks on the pixel intensity information in an area of the image. The most appropriate type of neural network, its ability to work with cells in a complex patterned background, and the accuracy of classification need to be assessed. Classification by direct application of neural networks has the potential for much faster cell image processing. We report on our progress in investigating this method of direct classification.

IMAGES

Sample images were acquired from a histologic source of considerable complexity. The nature of this complexity was in the number or type of cells to be recognized and in the background. The tissue under examination was from a 14-day inflammatory reaction to implantation of kangaroo tail tendon into rabbit paravertebral muscle. The histologic sections were embedded in paraffin, sectioned, and stained with hematoxylin and eosin. Figure 1 shows examples of the different cell types from the materials at the original resolution obtained as described below.

The slides were imaged with a commercially available image analysis system. This system comprised a Nikon

Eclipse E800 (Nikon Instech, Kanagawa, Japan) microscope with a PCO SensiCam 12-bit cooled color CCD camera (PCO Computer Optics GmGH, Kelheim, Germany). Control of image capture was done with SensiControl 4.03 software supplied with this camera.

The size of the images captured was $1,280 \times 1,024$ pixels, saved in a bit-map (.bmp) format. Calibrated scale rulers in x and y directions were captured at the same time as the sample images. The size of one pixel in the images as calculated from these calibration rulers is approximately 130×130 nm. The Sensicam red, green, and blue (RGB) color filter set produces a blue band from 400 to 575 nm, with a peak relative sensitivity of 0.7 at about 450 nm. The blue band crosses over with the green band at approximately 495 nm, with a relative sensitivity of 0.32. The green band extends from 455 to 640 nm, with a peak relative sensitivity of 1.0 at about 540 nm. The green band crosses over with the red band at 580 nm, with a relative sensitivity of 0.42. The red band covers the spectrum from 550 to 700 nm, with a peak relative sensitivity of 0.95 near 620 nm.

METHOD

Neural networks under investigation include (a) a three-layer, fully connected, back-propagation architecture, (b) a four-layer, fully connected, back-propagation architecture, and (c) a two-layer, shared-weights architecture (15,16). Figure 2 shows the basic architectures of the neural networks used in this study.

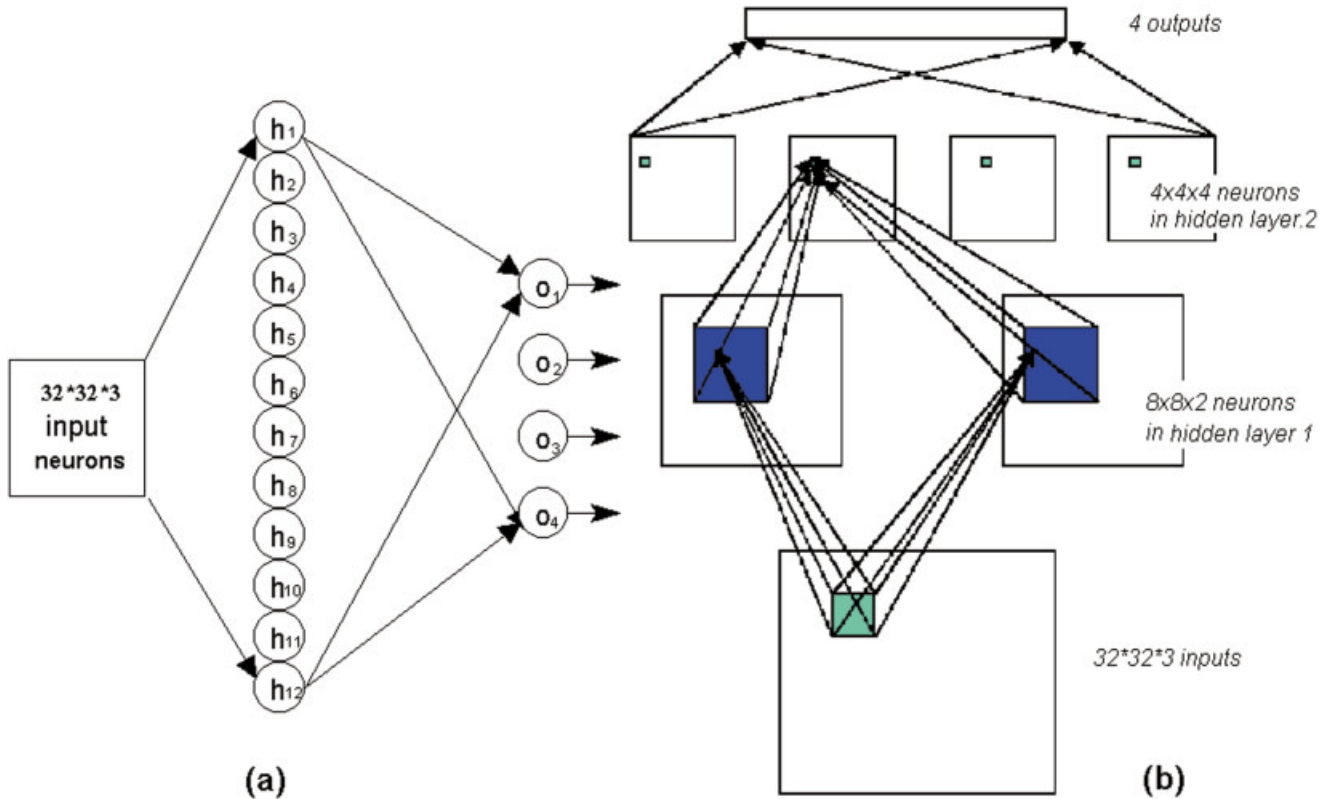


FIG. 2. Basic structures of the neural networks in this study. **a:** Three-layer, fully connected, back-propagation neural network with 3,072 input neurons, 12 hidden-layer neurons, and four output-layer neurons. **b:** Two layers of shared-weights structure with 3,072 input neurons, 128 first hidden-layer neurons in two groups of 64, and 64 second hidden-layer neurons in four groups of 16, and four output-layer neurons. [Color figure can be viewed in the online issue, which is available at www.interscience.wiley.com.]

Figure 2a shows the three-layer, fully connected, back-propagation neural network. There are 3,072 input neurons in the input layer ($3,072 = 32 \times 32$ input image pixel matrix $\times 3$ colors for each pixel), 12 hidden neurons in the hidden layer, and four outputs in the output layer. This is a simple structure, with one hidden layer. The four-layer, fully connected, back-propagation neural network has similar a structure, with two hidden layers (12 and seven neurons) between the input and output layers. The numbers of the hidden neurons were chosen on the basis of trials with the training set to be as low as possible consistent with learning.

Figure 2b shows the four-layer, two-layer shared-weights, back-propagation neural network. There are 3,072 input neurons in the input layer and four output neurons in the output layer. These two layers are the same as the input and output layers in the three-layer structure shown in Figure 2a.

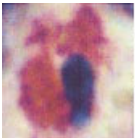
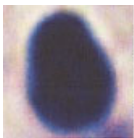
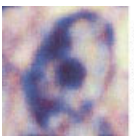
A training set and an independent test set of cells from each tissue sample were prepared and assessed manually by an independent expert for cell type (e.g., three types of sample cells shown in Table 1 are heterophil, lymphocyte, and macrophage).

The original images (1280×1024) were cropped to include only the object of interest (one cell in each

cropped frame) and then scaled down to form a 32×32 pixel frame containing each cell image. These scaled images were used as direct RGB inputs to the neural network. Image cropping was done by manually placing a selection window over a target object (cell) in the original image so that the cell was selected. Each pattern in the training and testing set consists of a pattern name, $32 \times 32 \times 3$ color pixel data, and a target output code. Test set cells are never used for training and used only for testing the performance of a trained neural network. Figure 3 illustrates the actual input, target, and output of cell patterns. The outputs from the neurons in the output layer of the neural network are presented in percentages, from 0% to 100%. With respect to the target outputs, "0" equals 0% and "1" equals 100%. The target outputs are defined as [0010] for heterophil, [0100] for lymphocyte, and [1000] for macrophage. All the patterns were manually classified by an expert to define the target output of the patterns.

The training set was manually selected to include only 25 easily recognizable cells of each type. The testing set consisted of the remainder. Figure 3 shows all the cell types used for training. The selected neural network was trained by the training patterns. The connection strengths were modified during the training to classify the three types of training patterns correctly. Then the testing set

Table 1
*Training and Testing Results From Rabbit Back Muscle**

No. cells	tr	te	Three-layer fully connected back-propagation NN					Four-layer fully connected back-propagation NN					Two hidden layers of shared-weight NN				
			Training (rate 100%)		Testing			Training (rate 100%)		Testing			Training (rate 100%)		Testing		
			tss	pss	Rate	tss	pss	Rate	tss	pss	Rate	tss	pss	Rate	tss	pss	Rate
25	26		0.09	0.0043	3.62	0.14	25/26 (96%)	0.09	0.0037	3.31	0.1184	24/26 (92%)	0.03	0.0012	1.63	0.0626	25/26 (96%)
		0010															
25	94		0.12	0.0060	0.74	0.07	91/94 (97%)	0.03	0.0011	4.61	0.0491	90/94 (95%)	0.01	0.0005	4.87	0.0518	91/94 (97%)
		0100															
25	85		0.11	0.0055	8.15	0.10	82/85 (96%)	0.04	0.0016	4.85	0.0571	82/85 (96%)	0.02	0.0006	3.03	0.0322	84/85 (99%)
		1000															
75	205	Total	0.40	0.0050	12.51	0.08	198/205 (97%)	0.15	0.0013	12.77	0.0465	196/205 (96%)	0.06	0.0013	9.53	0.0465	200/205 (98%)

*NN, neural network; pss, average sum square error for each cell; te, test set; tr, training set; tss, total sum square error.

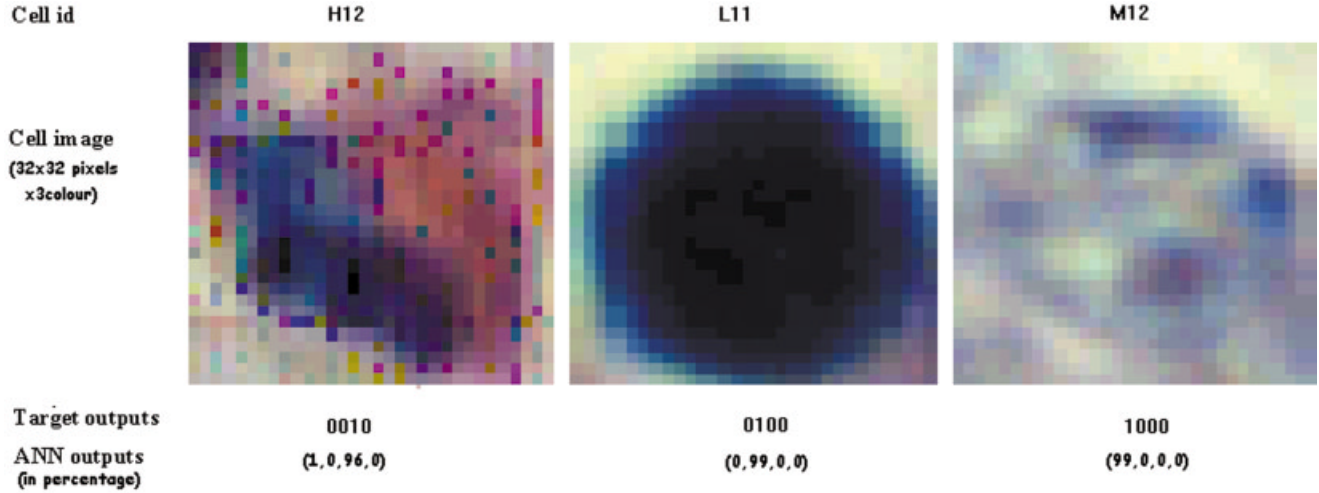


Fig. 3. Sample data from a neural network for the three types of cell. Each data set consists of input data (cell id, 32×32 pixel image, target output pattern) and the neural network output. [Color figure can be viewed in the online issue, which is available at www.interscience.wiley.com.]

was input into the neural network to test the classification rate of the trained neural network.

The output neurons of the ANN generate analog data. Figure 3 shows sample outputs consisting four integers, ranging from "0" to "99." The larger value of the integer implies a more active neuron.

A post-processing procedure is required to produce a classification result from the neural network. In this study, all the sample patterns had target outputs that were coded according to the classification by an expert. There are three steps involved in this post-processing.

- The sum of square errors (pss) was calculated when each pattern was presented. The equation for calculating the pss is as follows:

$$pss = \sum_i (t_{pi} - o_{pi})^2 \quad (1)$$

where the index p is the input pattern that is presented to the network, the index i is the index of the output neurons "1" to "4" in the output layer, and pss is the squared error of pattern p . T_{pi} is the target output of the neuron i in the output layer when the input pattern p has been presented, and o_{pi} is the output from the neuron i forwarded by the forward propagation when the input pattern p has been presented.

Next, the pss will be compared with a threshold to determine the class of the input pattern. The threshold of the pss is set as 0.5 during the testing. If the pss is less than 0.5, the network has classified the input cell. Otherwise ($pss \geq 0.5$), the ANN has not classified the input cell pattern.

For the new samples without expert classification of target output, another post-processing procedure is necessary to present a classification result. This post-processing has the following rules:

- **Peak output neuron:** There are four output neurons. According to the target codes, it is obvious that the first neuron will be active when macrophage pattern is recognized, the second neuron will be active when lymphocyte is presented, and the third neuron will be active when heterophil is presented. It is important to locate the active neuron to distinguish the specific cell pattern.

- If the peak output is over "50" and the other neurons have outputs less than "50," the cell type is classified to the cell type specified by the targets in the pattern.

- If there is more than one neuron with an output over "50," then the cell type can not be decided.

- Conversely, if there is no output value more than "50," then the cell should not be classified by the ANN even if one neuron has a value much higher than the others.

- For the entire set of cells, a parameter, tss ($tss = \sum_n pss$) is calculated, where tss is the sum of the pss values for the set of n cells.

RESULTS

The three-layer back-propagation neural network, the four-layer back-propagation neural network, and the four-layer plus two-layer shared-weights neural network were fully trained on the image sources. The four-layer, fully connected, structure did not perform as well as the three-layer one, and the four-layer plus two-layers shared-weights neural network had the best performance in the test.

Table 1 shows the results for all three neural networks. The number of training and testing patterns and of sample cell types are listed in the left part of the table. The training and testing error with classification rates are presented in the right part of the table. This part of the table is further sub-sectioned into three parts relating the results from the three different neural networks. In this table, the

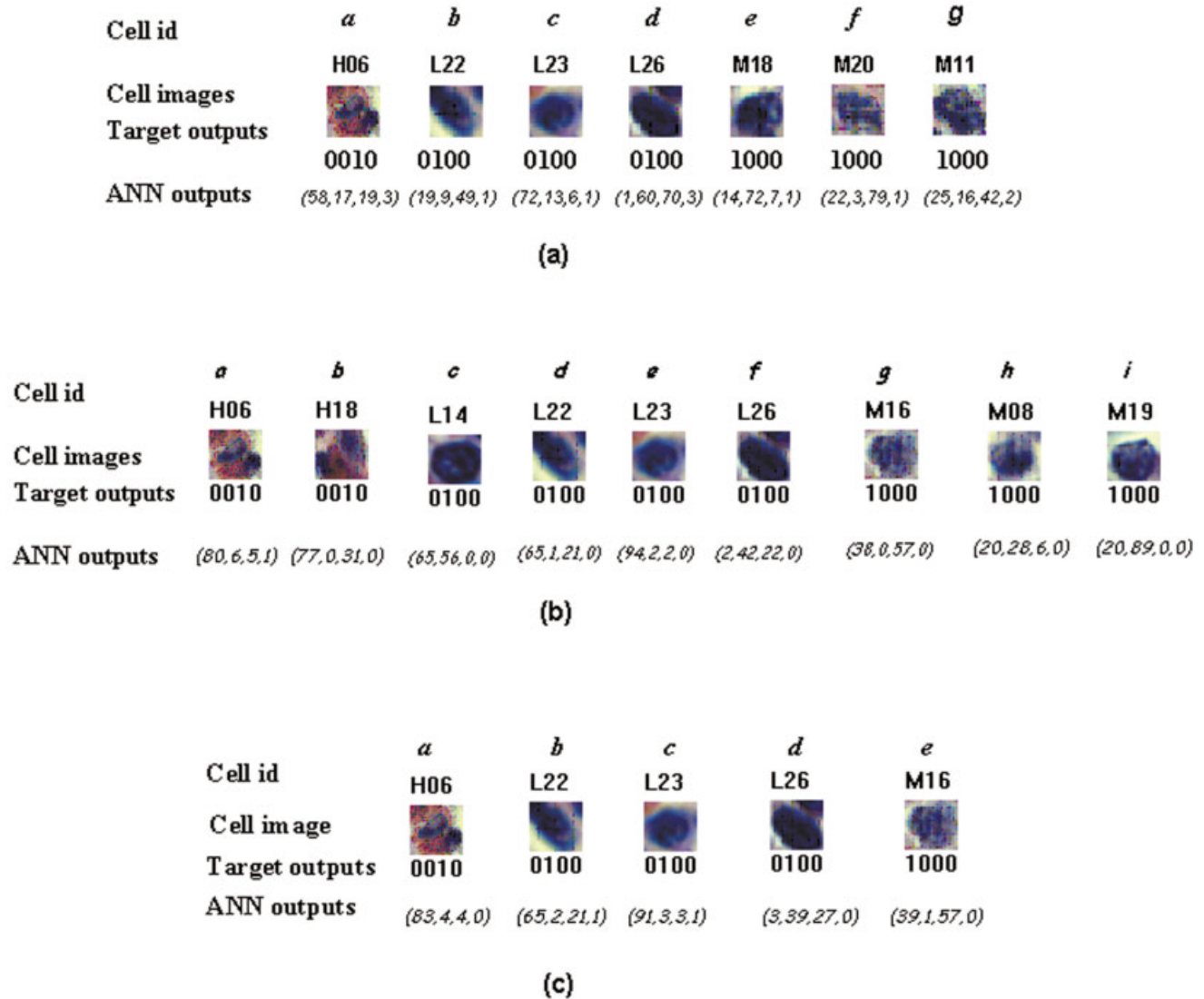


FIG. 4. Misclassified cells in the testing set. **a:** Misclassified cells from the three-layer back-propagation neural network: *a*, an H was misclassified as an M; *b*, an L was misclassified as an unknown cell; *c*, an L was misclassified as an M; *d*, an L was misclassified as an M; *e*, an M was misclassified as an L; *f*, an M was misclassified as an H; *g*, an M was misclassified as an unknown cell. **b:** Misclassified cells from the four-layer back-propagation neural network: *a*, an H was misclassified as an M; *b*, an H was misclassified as an M; *c*, an L was misclassified as an unknown cell; *d*, an L was misclassified as an M; *e*, an L was misclassified as an M; *f*, an L was misclassified as an unknown cell; *g*, an M was misclassified as an H; *h*, an M was misclassified as an unknown cell; *i*, an M was misclassified as an L. **c:** Misclassified cells from the two-layer shared-weights neural network: *a*, an H was misclassified as an M; *b*, an L was misclassified as an M; *c*, an L was misclassified as an M; *d*, an L was misclassified as an unknown cell; *e*, an M was misclassified as an H. H, heterophil; L, lymphocyte, M, macrophage. [Color figure can be viewed in the online issue, which is available at www.interscience.wiley.com.]

parameter *tss* is the total sum square error, and *pss* is the average sum square error for each cell.

Three kinds of cells (heterophil, lymphocyte, and macrophage) are presented for cell typing in the training and testing. From the left part of the table, 75 cells with 25 in each of three different kinds of cell are in the training set. Two hundred five cells are in the testing set, with 26, 94, and 85 in each corresponding cell type. The cells in the testing set were not the same cells as in the training set, but were selected to be the same types of cells as in the training set.

From the right side of the Table 1, the result for the three-layer ANN shows that seven cells were not correctly recognized by the three-layer back-propagation neural network. They are listed in Figure 4a. One heterophil, three lymphocytes, and three macrophages in the testing set were misclassified or non-classified. The direct classification rate was 97% for the entire test set cells, with 96%, 97%, and 96% for each cell type separately.

The results from the four-layer, fully connected, neural network are presented in the middle part of Table 1. There were nine cells that were not correctly

recognized by the neural network. They were two heterophils, four lymphocytes, and two macrophages and are shown in Figure 4b. The recognition rates for each type of cell were 92% for heterophil, 95% for lymphocyte, and 96% for macrophage. The total correct recognition rate was 96%.

The results from the four-layer with two hidden layers of shared-weights neural network are presented at the right side of Table 1. Five cells were not correctly recognized by the neural network—one heterophil, three lymphocytes, and one macrophage—and are shown in Figure 4c. The testing rates for each type of cells were 96% for heterophil, 97% for lymphocyte, and 99% for macrophage. The total correct recognition rate was 98%.

Figure 4 lists the details of misclassified cells, and the misclassification cases are stated after each figure. For example, cell H06 was not correctly classified in all three neural networks. The outputs from the neural networks were [58,17,19,3], [80,6,5,1], and [83,4,4,0] for the three-layer, the four-layer, and the shared-weights neural networks, respectively. According to the predefined classification rule, the neural networks classified cell H06 as a macrophage because the first neuron was the active neuron with a value over “50.” However, it had a target output of [0,0,1,0], active at the third position, indicating a manual classification result from an expert as a heterophil.

L26 was classified as an unknown cell by all the three neural networks. From the outputs [1,60,70,3] in Figure 4a, the three-layer neural network could not classify this cell into any of the three types of cells defined because it had two outputs that were over “50.” From the outputs of [3,39,27,0] and [2,42,22,0] shown in Figure 4b and 4c, it could not be classified because none of the outputs was over “50.”

There were three macrophages, M18, M20, and M11, that were not correctly classified by the three-layer neural network; three macrophages, M16, M08, and M19, that were not correctly classified by the four-layer neural network; and one macrophage, M16, that was misclassified by the shared-weights neural network.

DISCUSSION AND CONCLUSION

A classification accuracy of up to 98% (with two-layer shared-weight ANN) was achieved in this study. This shows that the direct classification with image pixel intensity data through ANN is possible, even with some background variation in the image. This compares favorably with a previous study in the same project using sequential morphologic methods, which included principal component transform, and color similarity transform, which had the correct classification rate of 86% (17). It is interesting to note that, in bladder cancer screening, Hurst et al. reported correct classification of up to 78% of test cells by using a neural network with direct input of gray pixel intensities (6). In cervical cancer screening, Romeo et al. reported a testing result of 10-15 of 20 correct classifications (50-75%) of the cervical samples when using ANN on seven preprocessed parameters (10). Auto-

mated tumor grading based on the analysis of four major morphometric features by ANNs were present, with the correct grading rates of over 90% (18). For standard image analysis, the range of classification accuracy is 60-95.7% in the literature (18-21).

There are cells shown in Figure 4 that were not correctly classified. It can be seen that cells H06, L22, L23, and L26 were misclassified in all three neural networks (three-layer, four-layer, and shared-weights neural networks). Some reasons for these discrepancies may be the specific appearance of the cell images and in particular:

- Compared with the other heterophils in the training set, H06 has two larger and lighter nucleus lobes, and the nucleus lobes are at the middle of the image frame. Light-blue chromatin clustered in the middle of the image frame is more typical for a macrophage nucleus, and this may explain the discrepancy from the neural network. H06 also does not contain much red cytoplasm.
- From the cell images of L22 and L23, for example, it is not difficult to observe that these lymphocytes have less dense nucleus as compared with the typical lymphocytes in the training set. Further, the lower density of nucleolus region is one of the most important features of a macrophage. This may be the reason why lymphocytes L22 and L23 were misclassified as macrophages by all of three neural networks. L26 was misclassified as a heterophil because it has a light nucleus on a pink background.

The sum square error pss value varies when each new sample cell is presented to a neural network. The cutoff threshold of the pss was preselected as “0.5.” Most of the samples had pss values less than “0.1,” and some of them were between “0.1” and “0.5.” All were in the correctly classified group; however, the samples with pss > “0.1” might have been classified into wrong group if the preselected threshold of “0.5” had been increased further. These samples presumably have some different features from the training samples according to the neural network. Further study into these samples may lead to improvements in the neural network performance. The specific features may be found in these cells and may be used to select training sets to generate better classification performance.

When unknown cells are presented to a trained ANN, the input cell will be classified by the neural network according to which of the four outputs is over a cutoff value of “50.” This was defined in the post-processing rule under Method. The selection of this threshold was based on the experience with the neural networks. Although this selection of the threshold value for neuron outputs proved to be satisfactory in this study, further investigation of this parameter may improve the neural network performance. If the pre-chosen threshold is too low, the wrong classification rate will be increase. In contrast, if the pre-chosen threshold is too high, it will increase the number of unclassified cell samples.

The study of why and how the misclassifications occurred is necessary, even though a high correct recogni-

tion rate of 98% was achieved. Previous studies also have misclassification cases; however, it is uncommon to find the explanations for those misclassifications. It will become even more important to understand how misclassification occurs as the number of cell types is increased in subsequent studies.

In manually selecting the cropping windows, we used only those cells that visually could be classified as one of the defined cell types. This is similar to a rough segmentation procedure, thus greatly restricting the identification target area from the whole image (cell + background) and simplifying the classification task. Automating selection window placement is another enhancement step that could be integrated into this study procedure. This will require further study, in particular for areas with cell overlapping or tight clustering.

This study features direct classification of cells from cell image pixel data without a feature extraction procedure. Traditionally, direct image pixel data as inputs to neural networks have been used widely for statistical pattern recognition of numeric data and general character recognition tasks (22,23). The input image data for the above studies were binary, and the window sizes generally were smaller (e.g., 16×16). Compared with those studies, the cell images used in this study are full color images containing three-color intensities, with each color having 8 bits/pixel on a 32×32 pixel window.

There are a few difficulties in the use of direct pixel data as inputs in this study, mainly because of the large amount of data for each image. For example, for a color image with a size of 32×32 pixels having three intensities (red, green, and blue), this image requires 3,072 neural network inputs. These input neurons were fully connected to the hidden neurons, with every hidden neuron in the next layer having 3,072 connections to it. In Figure 2a, the three-layer, fully connected, neural network "3072-12-4" has 12 hidden neurons in first hidden layer, and the connections between the input layer to the hidden layer amounted to 76,864. There were 48 connections between the hidden layer and the output layer. Thus there were 76,912 connections in this neural network, which had to be modified during the training procedure. This procedure required considerable processing power to validate the weights of all these connections in an iterative basis.

All 3,072 pixel intensities are used as input, because compressing information before inputting it into the neural network may lose vital information required for recognition. However, image compression is required when the computing power is limited, even though compression of the image will lose some information. In this particular study, an input image size of 32×32 was selected as the most suitable in light of the available computing power. It can be improved by using the original pixel data instead of the compressed image pixel data. How well this compressed 32×32 frame works as compared with the original pixel will need further examination when more powerful computing resources become available.

Although most of the cells in this study do not have obvious orientation problems, orientation of cells is often

a consideration (4). In this study, cells were randomly oriented in the images and could be classified without reorientation. The four-layer back-propagation neural network with two layers of shared weights performed the best in this study. The share-weights structure has built-in, shift-invariant, feature map layers in hidden layers 2 and 3 (H2 and H3). Each H2 neuron looks at a 3×3 patch of H1 neurons; and each H3 neuron looks at a 5×5 patch of H2 neurons. All the neurons within a feature map share the same input weights but have independent biases. Thus, there are only two distinct 3×3 weight vectors from H1 to H2, one for each feature map in H2, and there are four distinct 5×5 weight vectors from H2 to H3. Theoretically, this shared-weights structure can reduce distortion and orientation problems because shift-invariant feature maps force the same operation on different parts of the image. This performs an operation similar to a convolution procedure (24). This neural network structure worked slightly better than the other fully connected structures in this study. However, the other two neural network structures appeared to cope adequately with respect to cell orientation for the present study.

Although there were only three valid cell classification types in this study, the neural networks were set up with four output neurons. In training, the fourth output value was set to zero for the target outputs. One would expect properly classified test set cells to have a zero or very low value for the fourth output. This occurred most of the time, but some test outputs had significant values for the fourth output, indicating that classification is less reliable. The use of an extra output prevents the ANN from being constrained into making a choice among the main classification types.

In this study, ANNs performed to a very high accuracy (up to 98% classification rate). Direct input of image pixel information without image segmentation and feature extraction is applicable. Neural networks have the potential to process a large amount of image data and classify the cells.

Further investigations involving automating cell selection and cropping, increasing the number of classification types (i.e., cell types), and analysis of misclassification results have been identified as areas of future research that may achieve a clinical application potential.

ACKNOWLEDGMENTS

We thank the Australian Key Centre for Microscopy and Microanalysis, in Sydney University, for providing access to the equipment for image capturing in the study and the Department of Haematology, Prince of Wales Hospital, Sydney, for providing the blood smears.

LITERATURE CITED

1. Mellors RC, Ortega LD. Analytical pathology. I. Histochemical demonstration of antibody localization in tissues, with special reference to the antigenic components of kidney and lung. *Lab Invest* 1955;4: 69-89.
2. Mellors RC, Arias-Stella J, Siegel M, Pressman D. Analytical pathology. II. Histochemical demonstration of glomerular-localizing antibodies in experimental glomerulonephritis. *Am J Pathol* 1955;31:687-715.

3. Mellors RC, Siegel M, Pressman D. Analytical pathology. III. New observations on the pathogenesis of glomerulonephritis, lipid nephrosis, periarteritis nodosa, and secondary amyloidosis in man. *Am J Pathol* 1955;32:455-499.
4. Sjostrom PJ, Frydel BP, Wahlerg LU. Artificial neural network-aided image analysis system for cell counting. *Cytometry* 1999;36:18-26.
5. Lo SB, Chan H, Lin J. Artificial convolution neural network for medical image pattern recognition. *Neural Netw* 1995;8:1201-1214.
6. Hurst RE, Bonner RB, Ashenayi K, Veltri RW, Hemstreet III GP. Neural net-based identification of cells expressing the p300 tumor-related antigen using fluorescence image analysis. *Cytometry* 1997;27:36-42.
7. Schluter N, Heygster G. Remote sensing of Antarctic clouds with infrared and passive microwave sensors. *Meteorolog Z* 2002;11:21-36.
8. Foody GM, Cutler ME, McMorrow J, Pelz D, Tangki H, Boyd DS, Douglas I. Mapping the biomass of Bornean tropical rain forest from remotely sensed data. *Global Ecol Biogeogr Lett* 2001;10:379-387.
9. Kok MR, Boon ME, Schreiner-Kok PG, Hermans J, Grobbee DE, Kok LP. Less medical intervention after sharp demarcation of grade 1-2 cervical intraepithelial neoplasia smears by neural network screening. *Cancer Cytopathol* 2001;93:173-178.
10. Romeo M, Burden F, Quinn M, Wood B, McNaughton D. Infrared microspectroscopy and artificial neural networks in the diagnosis of cervical cancer. *Cell Mol Biol* 1998;44:179-187.
11. Godavarti M, Rodriguez JJ, Yopp TA, Lambert GM, Galbraith DW. Automated particle classification based on digital acquisition and analysis of flow cytometric pulse waveforms. *Cytometry* 1996;24:330-339.
12. Boon ME, Beck S, Kok LP. Semiautomatic PAPNET analysis of proliferating (MiB-1-positive) cells in cervical cytology and histology. *Diagn Cytopathol* 1995;13:423-428.
13. Ruggeri A, Pajaro S. Automatic recognition of cell layers in corneal confocal microscopy images. *Comput Methods Programs Biomed* 2002;68:25-35.
14. Berger P, Lavallec J, Rouiller R, Laurent F, Marthan R, Tunon-De-Lara JM. Assessment of bronchial inflammation using an automated cell recognition system based on colour analysis. *Eur Resp J* 1999;14:1394-1402.
15. McClelland JL, Rumelhart DE. Explorations in parallel distributed processing: a handbook of models, programs and exercises. Cambridge: MIT Press; 1986.
16. Fausett LV. Fundamentals of neural networks: architectures, algorithms, and applications. Saddle Brook, NJ: Prentice-Hall; 1994.
17. Vafaadust M. Computerised cell recognition in histology of biomaterials [DPhil thesis]. Sydney: University of New South Wales; 1994.
18. Kolles H, Wangenheim AV, Rahmel J, Niedermayer I, Feiden W. Data-driven approaches to decision making in automated tumor grading: an example of astrocytoma grading. *Anal Quant Cytol Histol* 1996;18:298-304.
19. Cseke I. A fast segmentation scheme for white blood cell images. Paper presented at the International Conference on Pattern Recognition; The Hague, Netherlands; 1992.
20. Revenu M, Elmoataz A, Porquet C, Cardot H. An automatic system for the classification of cellular categories in cytological images. *SPIE Intell Robots Comput Vis XII* 1993;2055:32.
21. Walts AE, Morimoto R, Marchevsky AM. Computerized interactive morphometry and the diagnosis of lymphoid-rich effusions. *Am J Clin Pathol* 1993;99:570-575.
22. Arica N, Yarman-Vural FT. An overview of character recognition focused on off-line handwriting. *IEEE Trans Syst Man Cybernet C Appl Rev* 2001;31:216-233.
23. Jain AK, Duin RPW, Mao J. Statistical pattern recognition: a review. *IEEE Trans Pattern Anal Mach Intell* 2000;22:4-37.
24. Gedeon TD, Mann GA. *Comp4444 neural networks*. Sydney: School of Computer Science and Engineering, University of New South Wales; 1994.